IET Renewable Power Generation

Special Issue Call for Papers

Be Seen. Be Cited.
Submit your work to a new IET special issue

Connect with researchers and experts in your field and share knowledge.

Be part of the latest research trends, faster.

Read more

The Institution of Engineering and Technology

Received: 27 February 2021 | Revised: 7 August 2021 | Accepted: 13 August 2021

IET Renewable Power Generation

DOI: 10.1049/rpg2.12279

The Institution of Engineering and Technology WILEY

ORIGINAL RESEARCH PAPER

Numerical calculation and model experiment of a novel external buoy type wave energy converter for navigation lighted buoys numerical study of a novel wave energy converter

Shuo Huang[1,2] | Weiqi Liu[1,2] | Chao Zhang[3] | Songwei Sheng[4] | Yage You[4] | Zhenpeng Wang[4] | Kaisheng Wen[1,2]

[1] School of Marine Engineering and Technology, Sun Yat-sen University, Zhuhai, China

[2] Southern Marine Science and Engineering Guangdong Laboratory (Zhuhai), Zhuhai, China

[3] Henan University of Technology, Henan, China

[4] Guangzhou Institute of Energy Conversion, Chinese Academy of Science, Guangzhou, China

Correspondence
Chao Zhang, Henan University of Technology, Henan 450001, China.
Email: zcjd@haut.edu.cn

Funding information
National Key Research and Development Program, Grant/Award Number: 2019YFB1504403; Department of Natural Resources of Guangdong Province, Grant/Award Number: GDNRC [2020]015; High-level Talent Fund of Henan University of Technology, Grant/Award Number: 2019BS016

Abstract

A novel external buoy type wave energy device with hydraulic conversion system used for navigation lighted buoys, named floating external double buoys wave energy device, is put forward and investigated by numerical calculations and model experiments. The hydrodynamic performance of the device under regular waves is numerically calculated based on linear potential flow theory and boundary element method. The generalized modal method is used to solve the hydrodynamic problems of multi-buoy with hinged constraints. The model experiments are carried out in a 2D wave tank with a depth of 0.9 m. The wave height is set to 1/40 of the wavelength. The influence of wave period and damping loads on the hydrodynamic performance of the device is tested. The results of numerical calculations and model experiments have shown that the appropriate selection of hydraulic damping coefficient is of great significance to improve the capture width ratio of the device, and this device has good capture performance in a certain wave range, and it is expected to effectively solve the problem of continuous power supply for middle and small types of navigation lighted buoys.

1 | INTRODUCTION

With the decreasing of petroleum resources, renewable energy is playing an increasingly important role in the energy structure. As one kind of renewable energy source, wave energy has the advantages of wide distribution and long persistence and is bound to be an important part of the future energy supply. Research and development programs on wave energy extraction have been carried out in most countries, such as the USA, Australia, Europe, Norway, and Japan [1–4]. Thousands of patents were granted on how to absorb wave energy and convert it to electricity or other forms of energy. Wave energy device is currently used in two ways: The installations above 100KW are used for utilities, such as power supply for offshore oil and gas platforms which have very high-power demands [5] or islands, and small installations below 50KW are mainly used for aquaculture, defence, marine monitoring and guiding [6].

In the past, there is no continuous power supply for navigation lighted buoys, which means they can't work for a long time unless replacing the battery. However, the need to replace the battery is the main reason leading to the increase in operation and maintenance costs. This situation is not addressed until the small wave energy converters (WECs) are proposed as an energy supply for the navigation light buoys [7]. Whittaker et al. [8–10] designed a Wells, self-rectifying turbine. The preliminary sea trials have shown that this simple turbine-generator set operates satisfactorily in wave powered navigation buoys of the current design. Blažauskas et al. [11] provided an overview of linear generator development and testing experience of three different prototype solutions applicable for small-scale wave energy

converters, such as attaching a linear generator to a Single Point Mooring Buoy to provide an additional source of energy for marine navigation signs. NAGATA et al. [12] designed and installed an OWC on navigation lighted buoy. Dunn et al. [13] described 'LAN', a geospatial data set that documents the development of coastal lights that guided ships around England and Wales from medieval times to 1911 and the number of navigation lights (all types) reported by benchmark period in LAN have reached 551 in 1911. In the mid-1980s, Guangzhou Institute of energy, Chinese Academy of Sciences successfully developed a 10 w Wells turbine WEC [14,15]. After more than ten years of development, there are many types of products and many improvements, such as BD-102G [16]. At present, more than 600 sets of those products are used in China's coastal areas and exported to Japan and other countries. The commercialization of type BD-102G WEC [17] illustrated the successful use of wave energy on navigation lighted buoys. With the development of water transportation and the increase of various types of navigation lighted buoys, the navigation lighted buoys have further requirements for the stability and efficiency of energy supply, on condition that maintenance funds and human resources are limited [18]. The small wave energy device designed for navigation lighted buoys need to be upgraded.

Generally, the wave energy device consists of two parts: the energy capture system and the energy conversion system. According to the working principle of capturing wave energy, WEC could be classified into three categories: Oscillating Bodies (OB), Oscillating Water Column (OWC) and Overtopping [19]. OB devices absorb wave energy through relative motions between different parts of the device, such as Power Buoy, Duck, Oyster, Pelamis, and the Sharp Eagle [20–26]; OWC devices absorb wave energy in a way that wave pushes and draws air through a turbine and turbine drive generators to generate electricity, such as Limpet in England [27]; Overtopping devices convert wave energy to gravitational potential and produce electricity through a turbine, such as Wave Dragon and Wave Cat [28, 29]. The energy conversion system of the wave energy device can be divided into four kinds: linear motor, hydraulic motor [30, 31], turbine, and mechanical conversion. OWC and Overtopping devices through the turbine transform compressed air or water energy into electricity, while OB devices are achieved through the other three ways.

The offshore floating wave energy device put forward in the present paper, named floating external double buoys wave energy device belongs to OB devices. This device consists of an absorption buoy, underwater substrate, and hydraulic system. The hydraulic system consists of a low-pressure tank, high-pressure accumulator, hydraulic motor, generator, and hydraulic cylinder. The absorption buoy and the underwater substrate are interconnected by hinge, and can rotate around the articulation point to produce relative motion.

The energy capture efficiency of this device depends strongly on the relative motion between the absorption buoy and the underwater substrate. The motion response of such system can be predicted during the design stages, and the key of it is to model the multi-body hinged by rigid constraints, which requires the representation of the constrained multi-body dynamics. There are two mainly methods that the researchers use to tackle this. One is the Lagrange multiplier method [32]. Sanghwan Heo et al. [33] studied the merits of the augmented formulation based on the Lagrange multiplier method for calculating the rotational motion of the floats considering the constraint forces. The results indicated that the validity of this method is verified, and is more efficient than the classic method. The other is the generalized modal method. Newman et al. used the generalized modal method to study the effect of elastic stiffness on the motion response of the system and the interaction between waves and clamped polyhedral boxes with hinges [34, 35]. As discussed by Taghipour and Moan [36], using the mode expansion technique can reduce the amount of calculation and storage, because fewer radiation problems need to be considered. What's more, the generalized modal method has the advantages that it is easy to program. According to its advantages, the generalized modal method, is used to analyse the device in this paper.

In the present paper, the hydrodynamic performance of the floating external double buoys wave energy device is investigated by numerical calculations as well as model experiments, and the optimal damping and the suitable wave period range of this device are found.

2 | NUMERICAL MODELLING METHOD

By assuming the water is homogenous, incompressible and with no viscosity, the flow is irrotational, and the fluid and buoys motions are small, the linear potential flow theory can be applied. The fluid and the buoys have the harmonic motions under the incident wave with the circular frequency ω, and then all the time-dependent quantities can be separated. The space velocity potential ϕ can be further decomposed into:

$$\phi(x,y,z) = \phi_I + \phi_D - i\omega \sum_{j=1}^{n} \xi_j \phi_j \tag{1}$$

here, ϕ_I, ϕ_D and ϕ_j are, respectively, the incident wave velocity potential, the wave diffraction velocity potential, and the radiation velocity potential that occurs when the buoys oscillate at unit speed. i indicates the imaginary part. n indicates the amount of motion components. ξ_j is the j motion displacement of the buoys in the frequency domain.

The incident wave velocity potential $\phi_I(x, y, z)$ under limited water depth is as follows:

$$\phi_I(x,y,z) = \frac{-igA}{\omega} \frac{\cosh[k(z+h)]}{\cosh(kh)} e^{ikx} \tag{2}$$

here, g is gravity acceleration; A is incident wave amplitude; h is the water depth; k is the wave number, and the wave number k meets the dispersion relationship $\omega^2 =$ gktanh(kh) under the limited water depth.

The diffraction velocity potential $\phi_D(x, y, z)$ and the radiation velocity potential $\phi_j(x, y, z)$ are expressed in $\phi_l(x, y, z)$ below, which satisfies the following definite conditions:

In the calculation domain:

$$\nabla^2\phi_I = 0 \tag{3}$$

Free surface S_F boundary condition:

$$\frac{\partial\phi_l}{\partial z}|_{z=0} - \frac{\omega^2}{g}\phi_l = 0 \tag{4}$$

Seabed surface S_D boundary condition:

$$\frac{\partial\phi_l}{\partial n}|_{z=-h} = 0 \tag{5}$$

Object surface S_w boundary condition:

$$\frac{\partial\phi_j}{\partial n} = n_j, \frac{\partial\phi_D}{\partial n} = -\frac{\partial\phi_I}{\partial n} \tag{6}$$

Finite radiant surface S_L boundary condition:

$$\begin{aligned}\phi_l(r,\theta,z) = &\left[c_0 H_0^{(1)}(kr) + \sum_{m=1}^{\infty} H_m^{(1)}(kr)\right.\\ &\left.\times\left(a_{0m}\cos m\theta + b_{0m}\sin m\theta\right)\right]\frac{\cosh\left[k\left(z+h\right)\right]}{\cosh(kh)}\\ &+\sum_{n=1}^{\infty}\left[c_n K_0^{(2)}(k_n r) + \sum_{m=1}^{\infty} K_0^{(2)}(k_n r)\right.\\ &\left.\times\left(a_{nm}\cos m\theta + b_{nm}\sin m\theta\right)\right]\frac{\cos\left[k_n\left(h+z\right)\right]}{\cos(k_n h)}\end{aligned} \tag{7}$$

$$\begin{aligned}\frac{\partial\phi_l}{\partial n} = &k\left[c_0\left(-H_1^{(1)}(kr)\right) + \sum_{m=1}^{\infty}\left(\frac{H_{m-1}^{(1)}(kr) - H_{m+1}^{(1)}(kr)}{2}\right)\right.\\ &\left.\times\left(a_{0m}\cos m\theta + b_{0m}\sin m\theta\right)\right]\frac{\cosh\left[k\left(z+h\right)\right]}{\cosh(kh)}\\ &+\sum_{n=1}^{\infty} k_n\left[c_n\left(-K_1(k_n r)\right) + \sum_{m=1}^{\infty}\left(\frac{-K_{m-1}(k_n r) - K_{m+1}(k_n r)}{2}\right)\right.\\ &\left.\times\left(a_{nm}\cos m\theta + b_{nm}\sin m\theta\right)\right]\frac{\cos\left[k_n\left(h+z\right)\right]}{\cos(k_n h)}\end{aligned} \tag{8}$$

here, $H_m^{(1)}(m = 0, 1, \cdots, \infty)$ is the first type of Hankel function, corresponding to the time factor $e^{-i\omega t}$ to form the outer wave and the subscript m represents the order; K_m is the second type of modified Bessel function, and $K_m(k_n r)$ exponentially decreases with the r increase, so the item associated with $K_m(k_n r)$ is the local disturbance wave; a_{nm} $b_{nm}$and $c_{nm}(n = 1, 2, \cdots, \infty; m = 1, 2, \cdots, \infty)$ are the complex coefficients to be determined.

The radiant surface S_L is a cylindrical surface, which surrounds the oscillating buoys and takes the z-axis as the centre at a limited distance. The interior of the cylinder is the computational domain.

The boundary integral equation satisfying the above defined conditions (3)–(8) was established by the boundary element method as follows:

$$\frac{\alpha}{4\pi}\phi_l(p) = \iint_s\left[\phi_l(p)\frac{\partial G(p,q)}{\partial n} - G(p,q)\frac{\partial\phi_l(p)}{\partial n}\right]ds \tag{9}$$

here, α the stereo angle of the surface corresponding to a point. S is the boundary surfaces of the entire computational domain and can be written as $S = S_F + S_D + S_w + S_L$; $G(p, q) = -\frac{1}{4\pi r_{pq}}$ is the simple Green function and r_{pq} is the distance from the field point p to the source point q on the boundary surfaces.

The boundary integral Equation (9) is discrete by the constant panel method [37] and can be written as follows:

$$[E_{pq}]\phi_l = [F_{pq}]\frac{\partial\phi_l}{\partial n}(p, q = 1, 2\cdots N) \tag{10}$$

here, the coefficient matrix $E_{pq} = \delta_{pq} + E'_{pq}$, $E'_{pq} = \frac{1}{2\pi}\iint_{S_q}\frac{\partial}{\partial n}\frac{1}{r_{pq}}ds$, δ_{pq} is the Kronecker Delta Function; and the coefficient matrix $F_{pq} = \frac{1}{2\pi}\iint_{S_q}\frac{1}{r_{pq}}ds$, N is the number of panels. By solving the linear Equation (10), the velocity potential on the object surface S_w can be obtained.

The wave excitation force f_{0k} caused by the incident velocity potential ϕ_I and the diffraction velocity potential ϕ_D on the device in the k-mode motion direction is as follows:

$$f_{ok} = \iint_{S_w} i\rho\omega(\phi_I + \phi_D)n_k ds \tag{11}$$

The radiation force F_k^R on the float can be expressed in terms of the additional mass and the radiation damping coefficient. Based on the generalized mode method:

$$\begin{aligned}F_k^R &= \int_{s_0}\mathrm{Re}\left[\rho\omega^2 e^{-i\omega t}\xi_j\phi_j\right]n_k ds\\ &= \mathrm{Re}\left[\rho\omega^2\xi_j e^{-i\omega t}\int_{s_0}\phi_j n_k ds\right]\\ &= \mathrm{Re}\left[\rho\omega^2\xi_j e^{-i\omega t}\int_{s_0}\left[\mathrm{Re}\left(\phi_j\right) + i\mathrm{Im}\left(\phi_j\right)\right]n_k ds\right]\\ &= \mathrm{Re}\left[\rho\omega^2\xi_j e^{-i\omega t}\int_{s_0}\mathrm{Re}\left(\phi_j\right)n_k ds\right]\\ &\quad+\mathrm{Re}\left[i\rho\omega^2\xi_j e^{-i\omega t}\int_{s_0}\mathrm{Im}\left(\phi_j\right)n_k ds\right]\end{aligned}$$

$$= -\rho \int_{s_0} \mathrm{Re}\left(\phi_j\right) n_k ds \cdot \mathrm{Re}\left[-\omega^2 \xi_j e^{-i\omega t}\right]$$
$$- \rho\omega \int_{s_0} \mathrm{Im}\left(\phi_j\right) n_k ds \cdot \mathrm{Re}\left[-i\omega \xi_j e^{-i\omega t}\right]$$
$$= -a_{jk}\ddot{x}_j - b_{jk}\dot{x}_j \tag{12}$$

here, a_{jk} and b_{jk} are, respectively, the additional mass and radiation damping produced by the *j*-mode motion of the device in the *k*-mode motion direction.$\dot{x}_j$ and $\ddot{x}_j$ are, obviously, the instantaneous velocity and acceleration. The expressions of them are as follows:

$$a_{jk} = \rho \iint_{S_w} \mathrm{Re}[\phi_j] n_k ds \tag{13}$$

$$b_{jk} = \rho\omega \iint_{S_w} \mathrm{Im}[\phi_j] n_k ds \tag{14}$$

$$\dot{x}_j(t) = \mathrm{Re}[-i\omega \xi_j e^{-i\omega t}] \tag{15}$$

$$\ddot{x}_j(t) = \mathrm{Re}\left[-\omega^2 \xi_j e^{-i\omega t}\right] \cdot \tag{16}$$

In the *j*-mode motion, the radiation velocity potential produces radiation force f_{jk}^R in the *k*-mode motion direction. Knowing that $F_k^R = \mathrm{Re}[f_{jk}^R e^{-i\omega t}]$, the radiation force f_{jk}^R in the frequency domain is obtained by separating the time factor *t*, and can be written as:

$$f_{jk}^R = (\omega^2 a_{jk} + i\omega b_{jk})\xi_j \tag{17}$$

Since the actual energy conversion process is complex and cannot be finely simulated in numerical calculations, only the effect of the external damping generated by the hydraulic system on the device is considered. The PTO system of WEC is typically modelled as a combination of a linear damping and a linear spring. As the mooring system is not considered, the total forces comprise the gravity of the device, wave force, elastic stiffness force, and external damping force [38]. In this paper, we study the relationship between the PTO damping and the conversion efficiency of this device to find the optimal damping, so the elastic stiffness is not the major concern and is set as zero [39, 40]. The external damping force F_k^f exists in the rotation direction [41] between the absorption buoy (floater1) and the underwater substrate (floater2) as shown in Figure 1, can be written as:

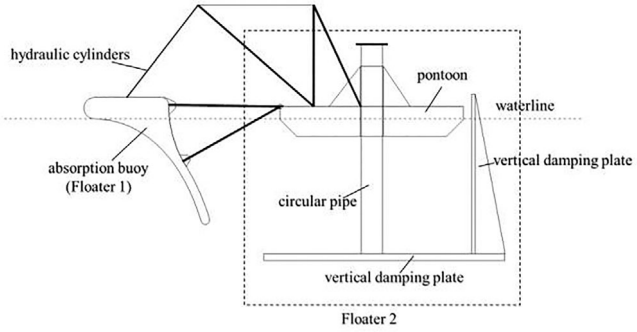

FIGURE 1 Schematic diagram of floating external double buoys wave energy device

$$F_k^f = C_{jk}^f \dot{x}_j \tag{18}$$

here, C_{jk}^f is the external damping coefficient matrix.

Based on the generalized mode method, the motion equation of the device in the frequency domain is obtained as follows:

$$(-\omega^2 M_{jk} - \omega^2 a_{jk} - i\omega b_{jk} - i\omega C_{jk}^f + C_{jk})\xi_j = f_{0k} \tag{19}$$

here, M_{jk} is the mass matrix, C_{jk}^f is the matrix of restoring force coefficients, the expressions of them are as follows:

$$M_{jk} = \begin{bmatrix} m_1 + m_2 & 0 & m_1(z_c^1 - z_0) & m_2(z_c^2 - z_0) \\ 0 & m_1 + m_2 & -m_1(x_c^1 - x_0) & -m_2(x_c^2 - x_0) \\ m_1(z_c^1 - z_0) & -m_1(x_c^1 - x_0) & I_{11}^1 + I_{33}^1 & 0 \\ m_2(z_c^2 - z_0) & -m_2(x_c^2 - x_0) & 0 & I_{11}^2 + I_{33}^2 \end{bmatrix} \tag{20}$$

$$C_{jk} = \begin{bmatrix} 0 & 0 & 0 & 0 \\ 0 & \rho g A_1 + \rho g A_2 & -\rho g I_1^{A_1} & -\rho g I_1^{A_2} \\ 0 & -\rho g I_1^{A_1} & \rho g(I_{11}^{A_1} + I_3^{V_1}) - m_1 g(z_c^1 - z_0) & 0 \\ 0 & -\rho g I_1^{A_2} & 0 & \rho g(I_{11}^{A_2} + I_3^{V_2}) - m_2 g(z_c^2 - z_0) \end{bmatrix} \tag{21}$$

$$\begin{cases} I_{11}^{1} = \iiint_{V_1} (x - x_0)^2 dm \\ I_{33}^{1} = \iiint_{V_1} (z - z_0)^2 dm \\ I_{11}^{2} = \iiint_{V2} (x - x_0)^2 dm \\ I_{33}^{2} = \iiint_{V_2} (z - z_0)^2 dm \end{cases}, \begin{cases} I_{1}^{A_1} = \iint_{A_1} (x - x_0) dxdy \\ I_{1}^{A_2} = \iint_{A_2} (x - x_0) dxdy \\ I_{11}^{A_1} = \iint_{A_1} (x - x_0)^2 dxdy \\ I_{11}^{A_2} = \iint_{A_2} (x - x_0)^2 dxdy \\ I_{3}^{V_1} = \iiint_{V_1} (z - z_0) dV \\ I_{3}^{V_2} = \iiint_{V_2} (z - z_0) dV \end{cases} \quad (22)$$

where $m_1$and m_2 are, respectively, the mass of the floater1 and floater2. (x_c^1, y_c^1, z_c^1) and (x_c^2, y_c^2, z_c^2) is the gravitational centre of floater1 and floater2, respectively. $(x_0,y_0,z_0)$is the hinge point between floater1 and floater2. V_1, $A_1$and V_2, $A_2$are the volume of displacement and waterplane area of floater1 and floater2 respectively.

When articulation is considered, the degrees of freedom of the floater1and the floater2 become 4. ξ_1 is the overall surge motion and ξ_2 is the overall heave motion. ξ_3 and ξ_4 are the pitch motion of the floater1 and the floater2 respectively. The power P_w absorbed by the device from the wave energy can be calculated by:

$$P_W = \frac{1}{T} \int_0^T F^f \dot{\theta} dt \quad (23)$$

where T is the wave period, $\theta = \xi_3 - \xi_4$ is the relative angular displacement, as well as the relative angular velocity $\dot{\theta} = \omega(\theta_i cos\omega t - \theta_R sin\omega t)$.

Thus, the power P_w can be express as:

$$P_W = \frac{1}{2}\omega^2 C^f (\xi_3 - \xi_4)\overline{(\xi_3 - \xi_4)} \quad (24)$$

here, $(\xi_3 - \xi_4)$ represents the complex conjugate of $\overline{(\xi_3 - \xi_4)}$.

The input power P_0 of the wave within the unit width is:

$$P_0 = [\pi h A^2 \rho g / \sinh(4\pi h/\lambda) + A^2 \rho g \lambda / 4]/T \quad (25)$$

The capture width ratio η is as follows:

$$\eta = \frac{P_W}{P_0 * b} \times 100\% \quad (26)$$

Here, b is the width of the device.

This numerical model has been validated in earlier work [42]. The correctness of the numerical models for the motion of rectangular and hemispherical bodies under waves is verified, by comparing the results in the literature with analytical solutions.

3 | NUMERICAL CALCULATION

The structure part of floating external double buoys wave energy device, as shown in Figure 1, consists of two main part: the absorption buoy and the underwater substrate, with a total width of 0.7 m, a total length of 3.6 m, a total height of 1.4 m, the draft of 0.74 m. This device is designed based on the "Sharp Eagle" WEC [43], using an absorption buoy with an eagle beak shape to capture wave energy and a novel underwater substrate is designed. The pontoon installed on the underwater substrate is 0.22 m long, 0.18 m high, and 0.7 m wide. The absorption buoy of the device is 0.7 m wide with the hydraulic conversion system as Power Take-Off (PTO) system.

In the case of the physical model corresponding to the real sea conditions, the device works as follows. After the floating device is subjected to waves, the relative pitch motion which is capable of capturing the wave energy, of the absorption buoy and underwater substrate around the hinge point is produced. The energy is absorbed by the rotation angle [44] difference between them around the hinge point. The hydraulic cylinder accordingly pumps the low-pressure oil into the high-pressure accumulator. When hydraulic energy accumulates to a certain pressure in the accumulators, high-pressure hydraulic oil will be released by automatic controllers to drive hydraulic motors, then generate electric power. Through the accumulator, the unstable wave energy can be converted into a relatively stable energy output. However, in addition to the wave energy capture motion, there are other modes of motion. The presence of other modal motions will cause the captured motion to weaken, which means that less energy will be captured by the device. Thus, when developing floating wave energy devices, attention should be paid to make the capture motion larger and weaken other ineffective motions of the device. The usual method is to use a stable underwater substrate [45]. To improve the stability of the underwater substrate, it is designed to be equipped with a pontoon. The pontoon of underwater substrate is hinged to the absorption buoy, and can slide up and down along the circular pipe in the centre to overcome the influence of tidal range.

The previous study indicates that the selection of external damping is of great important to improve the performance of this device. In order to figure out the optimal damping of this device under different working conditions, a series of numerical calculations are carried out. The working conditions we decided are that the incident wave is a regular wave with a height of 1 m, an incident angle of 0°, and a period range of 1.0–3.15s.

According to the calculation results, the maximum capture width ratio is defined as the optimal capture width ratio under the same wave period, and the corresponding external damping is the optimal damping. The optimal capture width ratio of it, as shown in Figure 2, can be obtained by properly optimizing the external damping when the water depth of 5 m and an incident wave angular frequency of 2.0–6.0 rad/s. It can be seen obviously from Figure 2 that the curve of the optimal capture width ratio is a bimodal curve over the entire wave period range, reaching the peak value of 79% in the wave period of 1.25 s and the other peak value of 48% in the wave period of 2.1 s. The optimal damping of this device for different wave period under the same working conditions represented above is also shown in Figure 3. It can be seen that the optimal damping of this device shows a trend that increases monotonically with the increase of wave period.

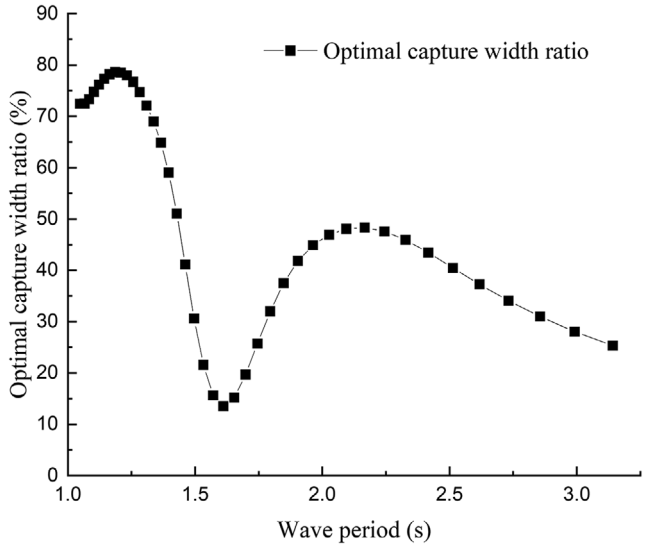

FIGURE 2 The optimal capture width ratio of floating external double buoys wave energy device

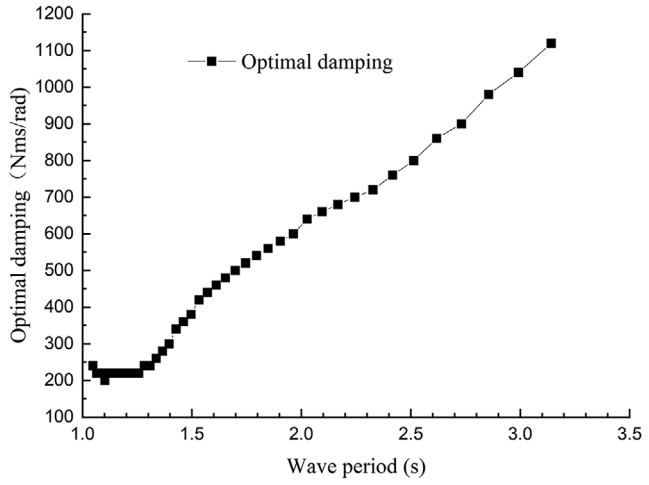

FIGURE 3 Optimal damping with different wave period

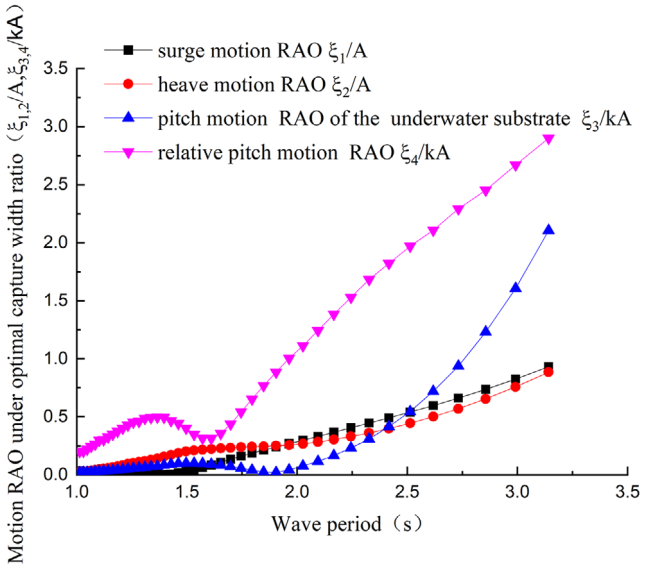

FIGURE 4 The motion response amplitude operator (RAO) of the device under optimal capture width ratio

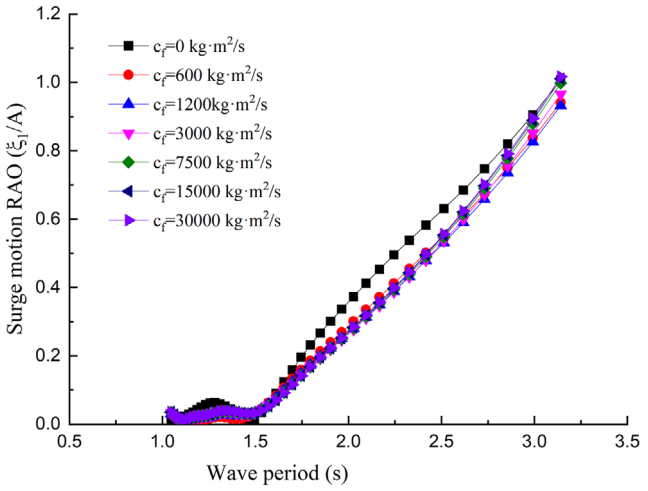

FIGURE 5 The overall surge motion RAO of the device

The motion RAO of this device corresponding to the optimal capture width ratio at different wave periods is shown in Figure 4. The displacement of surge and heave motion are both divided by the incident wave amplitude A to obtain dimensionless RAO in Figure 4. The pitch motion displacement is divided by the wave steepness kA to make it dimensionless.

Figure 4 shows that over the entire wave period range, as the wave period increases, the overall surge and heave motion RAO of this device gradually increases. Additionally, the pitch motion RAO of the underwater substrate is small and increases slowly until the wave period reaches 2.0 s. The relative pitch motion RAO is the difference between the pitch motion RAO of the absorption buoy and the underwater substrate. According to the curve of relative pitch motion RAO, the pitch motion displacement of the absorption buoy is always larger than that of the underwater substrate over the entire wave period range, and the relative pitch motion RAO has an extreme value in the wave period of 1.4 s.

The effect of the external damping coefficient on the motion of the device is shown in Figures 5–8. The overall surge motion and the overall heave motion are shown in Figures 5 and 6. The pitch motion of the underwater substrate can be seen in Figure 7, while the relative pitch motion among absorption buoy and underwater substrate can be seen in Figure 8.

As seen from Figures 5 and 6, with the increase of external damping, the change of the overall surge motion and heave motion RAO over the entire wave period range are small, within 1.2, which means the effect of external damping on those two motions are small.

Over the entire wave period range, the pitch motion displacement of the underwater substrate increases with the increase of wave period, as we can see from Figures 7 and 8.

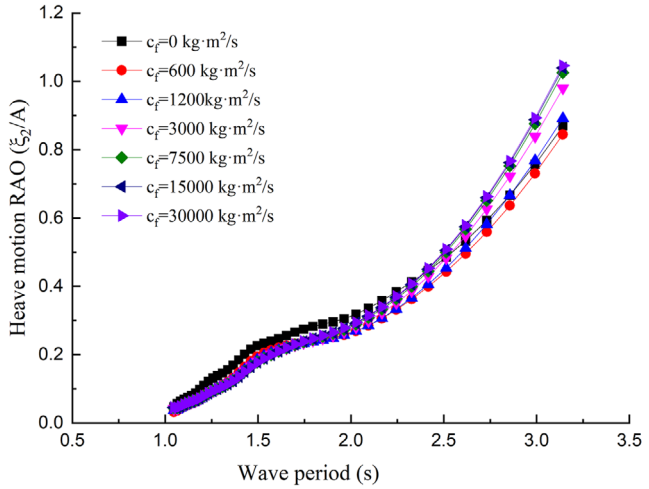

FIGURE 6 The overall heave motion RAO of the device

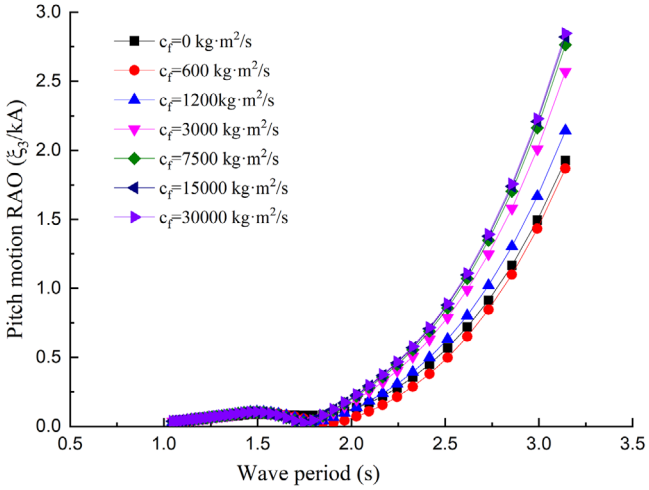

FIGURE 7 The pitch motion RAO of the underwater substrate

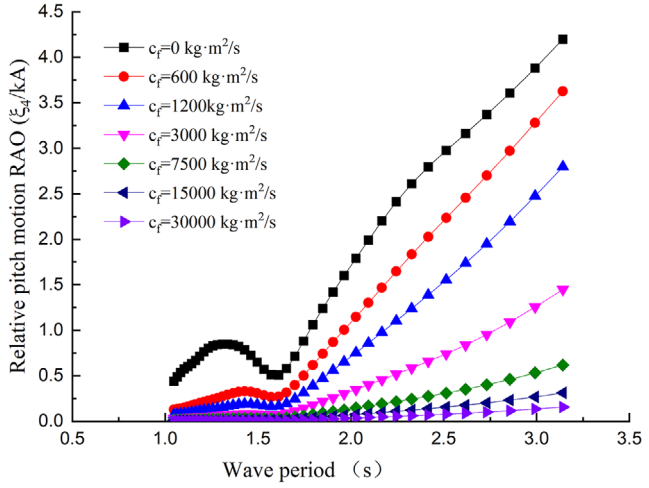

FIGURE 8 The relative pitch motion RAO

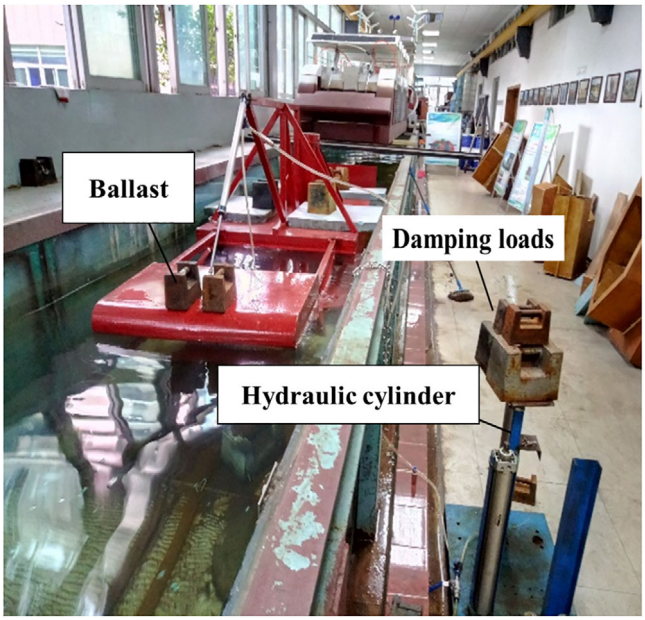

FIGURE 9 Test model

The relative pitch motion between the underwater substrate and absorption buoy decreases rapidly with the increase of the external damping coefficient, as we can see from Figure 8. This phenomenon is more pronounced after the wave period reaches 2.0 s. The reason is that the pontoon of the underwater substrate floats on the water surface, which increases the water-plane of the underwater substrate. When the external damping increases, the device is more likely to generate overall pitch motion under the wave excitation, and attenuate the relative pitch motion related to capturing wave energy. Under the same external damping conditions, the performance of the relative pitch motion is different with the different wave periods. When the relative pitch motion between the absorption buoy and the underwater substrate decreases, the ability of the hydraulic cylinder to convert the wave energy into hydraulic energy is also weakened simultaneously, which affects the performance of the device.

4 | MODEL EXPERIMENTS

To further study the performance and conversion efficiency of this device, the model experiment is conducted in a two-dimensional wave tank of Guangzhou Institute of energy, Chinese Academy of Sciences.

4.1 | Model parameters

The experiment is carried out in a two-dimensional wave tank with a depth of 0.9 m, as shown in Figure 9, and the parameters of the test model of floating external double buoys wave energy device are consistent with those in the numerical calculation. The main part of the test model is the underwater substrate,

TABLE 1 The regular wave parameters in experiments

Number	Wave period T (s)	Average wave height H (mm)
1	1.0	40
2	1.1	47
3	1.2	55
4	1.3	64
5	1.4	73
6	1.5	82
7	1.6	91

which is comprised of two parts: a pontoon and the damping plate. The other part of it is the absorption buoy with a width of 0.7 m, which is used to capture wave energy. The pontoon used as a buoyancy chamber with adjustable height to provide buoyance is 0.22 m long, 0.18 m high and 0.7 m wide. The hydraulic cylinder is respectively connected with the upper surface of the absorption buoy and the truss on the underwater substrate and captures the wave energy through the relative pitch motion of the absorption buoy and the underwater substrate. The floating state of the absorption buoy can be adjusted by placing a ballast weighing up to 10 kg on top of it. Additionally, the power P_w^* absorbed by the device in the model experiments is equivalent to the gravity power of the damping loads, and can be expressed as:

$$P_w^* = \frac{mgH}{t} \tag{27}$$

where m is the mass of damping loads, H is the displacement of the hydraulic cylinder.

According to the wave conditions in the South China Sea, we decide to take the wave height as 1/40 of the wavelength. The parameters corresponding to wave period and wave height of regular waves in experiments are shown in Table 1. The wave height recorder is set at 6 m in front of the device. The test results are subject to the measured wave parameters of the regular wave in Table 1.

4.2 | The optimal capture width ratio in experiments

During the model experiments, the optimal damping load over the entire wave period range, which can maximize the capture width ratio of the model can be found by changing the weight of the damping load on the hydraulic cylinder. The optimal capture width ratio corresponding to different loads (from 20 to 80 kg) for each period of the model experiment is measured, as shown in Figure 10.

The capture width ratio of the test model in each period, as seen from Figure 10, fluctuates slightly with the increase of the damping load. The capture efficiency of the model reaches the maximum and the capture width ratio is 39.3%, with the wave

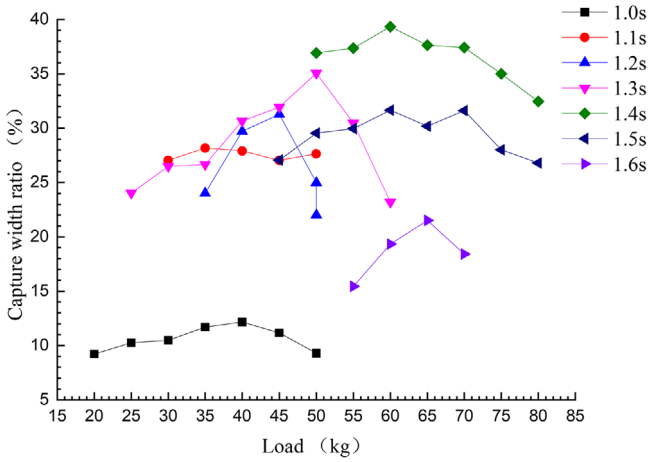

FIGURE 10 The capture width ratio of different loads in each period

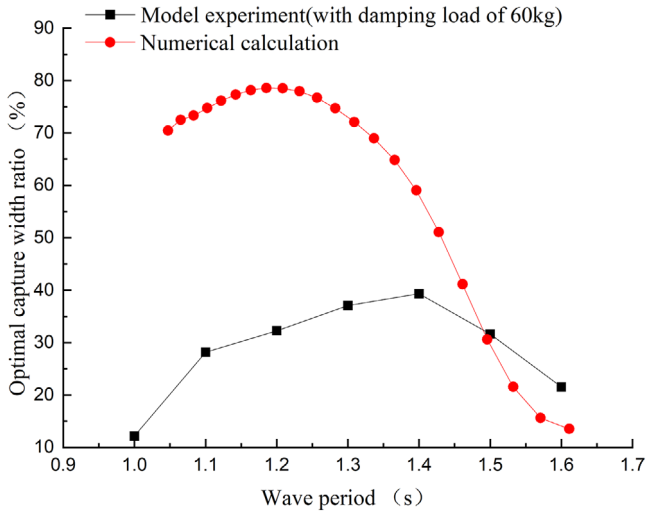

FIGURE 11 Optimal capture width ratio

height of 73 mm, the wave period of 1.4 s, and the mass of damping load of 60 kg. As a result, with the same wave condition, the damping loads with different mass will change the energy capture efficiency and the optimal capture width ratio.

The capture width ratio of the model experiments ranges from 30% to 40% under the wave period of 1.10–1.50 s, as we can see from Figure 11. The numerical results presented in the previous chapter show that the maximum capture width ratio of the device reaches 79% in the wave period of 1.25 s. This device performs well in the wave period range of 1.2–1.5 s, both in model experiments and numerical simulations.

5 | CONCLUSION

A novel external buoy type wave energy converter for navigation lighted buoys is proposed in this paper. Accurate and effective numerical calculation and model experiments are carried out to study the hydrodynamic performance of this device and to figure out the effects of wave period and working load on this

device. Based on the results of numerical calculation and model experiments, some conclusions about the wave energy device proposed in this paper are as follows:

1. Under different wave periods, the appropriate selection of hydraulic damping coefficient c_f is of great significance to improve the capture width ratio of those devices. As a result, the external damping coefficient corresponding to the high capture width ratio can be used as a basis for hydraulic system design. Different external damping coefficients have little effect on the overall surge motion displacement of the device. However, the external damping coefficient has a greater impact on pitch motion. As the increase of the external damping coefficient, the peak value gradually decreases.
2. According to the results of numerical calculation, the optimum capture width ratio of floating external double buoys wave energy device model reaches the peak value of 79% in the wave period of 1.25 s and the other peak value of 48% at a wave period of 2.10 s.
3. The results of model experiments showing that the maximum capture width ratio is 39.3% in the wave period of 1.40 s. Under the wave period of 1.10–1.50 s, the capture width ratio of it remains between 30% and 40%.
4. In addition to the optimization of the hydraulic system, the device has a suitable wave period range due to its own characteristics. The suitable wave period range of the model is 1.20–1.5 s. This device shows good performance within this period range, whether in the model experiments or the simulation calculations.

Generally speaking, floating external double buoys wave energy device has excellent capture performance in a certain wave range. Also, by adjusting the external damping, the capture performance of the device can be improved in a certain wave range, and has a good application prospect and can be expected to solve the problem of continuous power supply for middle and small types of navigation lighted buoys. However, the present study has some limitations. The friction of the hydraulic cylinder and the reflected waves from the flume sidewalls are not taken into account in the two-dimensional model experiments, while the coupled motion of the anchor chain and the device is not considered in the numerical calculation. We expect to conduct a 3D model experiment in the future to verify the results of the simulation and further study the performance of this device.

FUNDING

The authors acknowledge the financial support from the National Key Research and Development Program (2019YFB1504403), Special Fund for promoting high-quality economic development of province in 2020 from Department of Natural Resources of Guangdong Province (Grant No. GDNRC[2020]015) and High-level Talent Fund of Henan University of Technology (2019BS016).

ACKNOWLEDGEMENTS

The authors acknowledge the financial support from the National Key Research and Development Program (2019YFB1504403), Special Fund for promoting high-quality economic development of province in 2020 from Department of Natural Resources of Guangdong Province (Grant No. GDNRC [2020]015) and High-level Talent Fund of Henan University of Technology (2019BS016).

ORCID

Weiqi Liu https://orcid.org/0000-0001-7426-5632

REFERENCES

1. Bergdahl, L.: Review of research in Sweden. In: Proceedings of the Wave Energy Workshop, Cork, Ireland (1992)
2. Fredrikson, G.: IPS wave power buoy Mark IV. In: Proceedings of the Wave Energy Workshop, Cork, Ireland (1992)
3. Nielsen, K., Meyer, N.I.: The Danish Wave Energy Programme, third ed., EWEC, Patras,Greece (1998)
4. Officers of World Energy Council, Survey of Energy ResourcesInterim Update 2009, London, UK (2009)
5. Oliveira-Pinto, S., Rosa-Santos, P., Taveira-Pinto, F.: Assessment of the potential of combining wave and solar energy resources to power supply worldwide offshore oil and gas platforms. Energy Convers. Manage. 223, 113299 (2020)
6. Li, W.: Current situation analysis and future prospect of marine renewable energy technology development in China. In: China Renewable Energy Academic Conference, Kunming, Yunnan (2020)
7. Zhang, Y., Sheng, S., You, Y., Wang, K., Wang, Z.: Development Status and Application Direction of Wave Energy Generation Technology. Adv. New Renewable Energy 7(04), 374–378 (2019)
8. Whittaker, T.J.T., Folley, M.: Nearshore oscillating wave surge converters and the development of Oyster. Philos. Trans. R. Soc. London, Ser. A 370, 345–64 (2012)
9. Whittaker, T.J.T., McIlhagger, D.S., Barr, A.G.: Wells Turbines for navigation buoys. In: Twidell, J., Riddoch, F., Grainger, B. (eds.) Energy for Rural and Island Communities, pp. 289–297, Pergamon Press, Oxford (1984)
10. Whittaker, T.J.T., McIlhagger, D.S., Barr, A.G., Thompson, A.: Electrical considerations with wave powered navigation aids.: In: West, M., White, P., Duckers, L., Loughridge, B., Lockett, P., Peatfield, T. (eds.) Alternative Energy Systems, pp. 163–174, Pergamon Press, Oxford (1984)
11. Blažauskas, N., Pašilis, A., Knolis, A.: Potential applications for small scale wave energy installations. Renewable Sustainable Energy Rev. 49, 297–305 (2015)
12. Nagatas, S., Toyotak, K., Imai, Y., et al.: Experimental research on primary conversion of a floating OWC "Backward Bent Duct Buoy" In: The Seventeenth International Offshore and Polar Engineering Conference, Japan (2007)
13. Dunn, O.B., Alvarez-Palau, E.J.: Dataset for historical lighthouses and light aids to navigation (LAN). England and Wales, 1514–1911. Data Brief 31, 105991 (2020)
14. Yuan, W.: Research on the Utilization of Wave Energy for the Buoy Device. Dalian Maritime University, Dalian, China (2011)
15. Liang, X., Wang, W., Du, B.: Experimental research on performance of BBDB wave-activated generation device model. The Ocean Engineering 15, 77–86 (1997)
16. Liang, X., Yang, G., Wu, H.: Research on the BD102G type wave energy generation device for navigational buoy. Renewable Energy Resources, 32, 1933–1938. Chinese Academy of Sciences (2014)
17. Pan, G.: Research on Wave Energy Power Generation Device Applied to Navigation Mark. Zhejiang Ocean University, Zhejiang, China (2018)
18. Chen, L., Peng, G., Zhang, X.: The application and research of navigation-aids inspection and maintenance based on video surveillance. Procedia Eng. 15, 3088–3092 (2011)
19. Salter, S.H.: Wave power. Nature 249(5459), 720–724 (1974)
20. Solar Alliance.: 'pelamis'. Available at http://www.pelamiswave.com/pelamis-technology
21. Alves, M., Brito-Melo, A., Sarmento, A.: Numerical modelling of the Pendulum ocean wave power converter using a panel method. In: The Twelfth

International Offshore and Polar Engineering Conference, Kitakyushu, Japan (2002)
22. Henderson, R.: Design, simulation, and testing of a novel hydraulic power take-off system for the Pelamis wave energy converter. Renewable Energy 31(1), 271–283 (2006)
23. Yemm, R., et al.: Pelamis: Experience from concept to connection. Philos. Trans. R. Soc. London, Ser. A 370, 365–80 (2012)
24. Sheng, S.: Research on power take-off system of floating wave power device. J. Mech. Eng. 48(21), 141 (2012)
25. Henderson, R.: Design, simulation, and testing of a novel hydraulic power take-off system for the Pelamis wave energy converter. Renewable Energy 31(2), 271–283 (2006)
26. Henry, A. et al.: Advances in the design of the Oyster wave energy converter. In: Proceedings of the Royal Institution of Naval Architect's Marine and Offshore Renewable Energy Conference, London, UK (2010)
27. Voith.: 'Limpet.' Available at http://voith.com/corp-en/index.html
28. Kofoed, J.P., Frigaard, P., Friis-Madsen, E., et al.: Prototype testing of the wave energy converter wave dragon. Renewable Energy 31(2), 181–189 (2006)
29. Fernandez, H., Iglesias, G., Carballo, R., et al.: The new wave energy converter WaveCat: Concept and laboratory tests. Mar. struct. 29(1), 58–70 (2012)
30. He, X., Xiao, G., Hu, B., Tan, L., Tang, H., He, S., He, Z.: The applications of energy regeneration and conversion technologies based on hydraulic transmission systems: A review. Energy Convers. Manage. 205, 112413 (2020)
31. Sheng, W.: Wave energy conversion and hydrodynamics modelling technologies: A review. Renewable Sustainable Energy Rev. 109, 482–498 (2019)
32. Sun, L., Taylor, R.E., Choo, Y.S.: Responses of interconnected floating bodies. IES J. Part A: Civ. Struct. Eng. 4(3), 143–56 (2011)
33. Heo, S., Koo, W.: Numerical procedures for dynamic response and reaction force analysis of a heaving-point absorber wave energy converter. Ocean Eng. 200, 107070 (2020)
34. Newman, J.N.: Wave effective on deformable bodies. Appl. Ocean Res. 16(1), 47–59 (1994)
35. Lee, C.H., Newman, J.N.: An assessment of hydroelasticity for very large hinged vessels. J. Fluids Struct. 14(7), 957–970 (2000)
36. Taghipour, R.,.Moan, T.: Efficient frequency-domain analysis of dynamic response for the multi-body wave energy converter in multi-directional waves. In: Proceedings of 18th Offshore and Polar Engineering Conference, Vancouver, Canada. (2008)
37. He, W., Dai, Y.: The simple Green function technique for calculating the hydrodynamic forces acting on a body without forward speed. J. Hydrodyn. 7(4), 449–456 (1992)
38. Zhang, L., Jin, P., Zhou, B., Zheng, X., Liu, H.: Oscillation and conversion performance of double-float wave energy converter. J. Mar. Sci. Appl. 18(1), 54–63 (2019)
39. Zhang, H., Zhou, B., Vogel, C., Willden, R., Zang, J., Geng, J.: Hydrodynamic performance of a dual-floater hybrid system combining a floating breakwater and an oscillating-buoy type wave energy converter. Appl. Energy 259, 114212 (2020)
40. Zheng, Y., Liang, Z., Zhou, B., et al.: Analysis of the hydrodynamic performance of an oyster wave energy converter using Star-CCM+. J. Mar. Sci. Appl. 18, 153–159 (2019)
41. Chao, Z., Yage, Y., Aiju, C.: Hydrodynamics research of a two-body articulated wave energy device. Ocean Eng. 148, 202–210 (2018)
42. Chao, Z., Yage, Y., Wensheng, W., Yin, Y., Wang, Z.: Application of the modal method in the hydrodynamic calculations of wave energy devices. Acta Energiae Solaris Sinica 39(09), 2493–2498 (2018)
43. Sheng, S., You, Y., Wang, K. & Zhang, Y. : in: Research and development of sharp eagle wave energy convertor. In: 6th International Conference on Ocean Energy, Halifax, Canada (2014)
44. Zheng, S., Zhang, Y.: Analysis for wave power capture capacity of two interconnected floats in regular waves. J. Fluids Struct. 75, 158–173 (2017)
45. Carmichael, A.D.: An experimental study and engineering evaluation of the Salter Cam Wave energy converter (Report). NASA STI/Recon Technical Report N (1978)

How to cite this article: Huang, S., Liu, W., Zhang, C., et al: Numerical calculation and model experiment of a novel external buoy type wave energy converter for navigation lighted buoys numerical study of a novel wave energy converter. IET Renew. Power Gener. 15, 3385–3394 (2021). https://doi.org/10.1049/rpg2.12279